J Wood Sci (2018) 64:23–39
DOI 10.1007/s10086-017-1667-7

ORIGINAL ARTICLE

Performance evaluation of multi-storey cross-laminated timber structures under different earthquake hazard levels

Xiaofeng Sun[1] · Minjuan He[1] · Zheng Li[1] · Zhan Shu[1]

Received: 21 April 2017 / Accepted: 11 September 2017 / Published online: 25 October 2017

Abstract The inter-storey drift limitations are meaningful reference values for structural seismic performance evaluation. This paper presents an analytical investigation into the seismic performance of multi-storey cross-laminated timber (CLT) structures to obtain the drift limitations under different earthquake hazard levels reasonably. The Pinching4 model was used to simulate the nonlinear mechanical behavior of three types of connections used in CLT structures, and a numerical model was further developed to capture the lateral load-resisting properties of CLT shear walls. Moreover, three benchmark multi-storey CLT apartment buildings were designed using the Equivalent Static Force Procedure according to National Building Code of Canada (NBCC), and simplified structural models were developed for these buildings. Depending on the results from numerous time-history dynamic analyses, the empirical cumulative distribution functions (CDFs) of the maximum inter-storey drifts were constructed for the three benchmark buildings. The probability of non-exceedance (PNE) of inter-storey drift thresholds under different earthquake hazard levels was proposed and validated. It is recommended that for low-rise CLT buildings within three stories, values of 0.30%, 0.75%, and 1.40% can be considered as the drift limitations for frequent, medium, and rare seismic hazard levels, respectively. For mid-rise or high-rise buildings without three stories, 0.25%, 0.70%, and 1.30% can be considered as drift limitations.

✉ Zheng Li
zhengli@tongji.edu.cn

[1] Department of Structural Engineering, Tongji University, Shanghai 200092, China

Keywords Cross-laminated timber · Seismic performance evaluation · Inter-storey drift · Cumulative distribution function · Earthquake hazard level

Introduction

Cross-laminated timber (CLT), which was first developed in Austria and Germany about 20 years ago, is an innovative engineered wood product. According to the previous research conclusions and engineering experiences, such mass timber panelized system can be very competitive in residential or mixed occupancy middle-rise and high-rise buildings. Even for low-rise buildings, because of the high level of prefabrication, CLT structures can also provide a prospective alternative to the traditional timber-framing structures. The process of cross lamination can provide improved dimensional stability to the CLT panels that allow for prefabrication of long floor slabs and shear walls. Because the cross section of a CLT panel usually has three-to-five-glued layers of boards made up of solid timber or dimension lumber placed in orthogonally alternating orientation to the neighboring layers, it can provide high compressive strength and stiffness within the panel. Since the inherent nature of thick timber members to char slowly at a predictable rate, the massive wood systems are able to maintain significant structural capacity for extended durations when exposed to fire, which adds benefits to CLT structures. Due to the aforementioned advantages, CLT panelized system may offer a promising structural solution for the shift towards sustainable densification of urban centers in China in the future.

To obtain the mechanical properties of CLT panels and understand the failure modes of CLT structures, studies on CLT connections, wall or floor panels and the entire

structural systems have been conducted. For the studies on CLT connections, Gavric et al. [1, 2] tested the mechanical performance of hold downs angle brackets and screwed connections used for CLT panels, and an over-strength factor of 1.3 was approximated for hold downs and angle brackets. Moreover, an over-strength factor of 1.6 was provided for screwed connections. Schneider et al. [3, 4] defined the energy-based cumulative damage index for CLT connections. The relations between the damage index and physical connection damage were provided. For the studies on CLT wall panels, experimental results from Ceccotti et al. [5] indicated that connection layouts had significant influence on the overall behavior of CLT shear walls. Dujic et al. [6, 7] investigated the influence of boundary conditions and the values of vertical loads on the deformation mode and shear strength of CLT shear walls. Popovski et al. [8] investigated the influence of cyclic loading protocol and openings for windows and doors on the lateral performance of CLT shear walls. For the studies on the CLT structures, Ceccotti et al. [9, 10] evaluated the strength reduction factor for seismic design according to the results of shaking table tests on 3-storey and 7-storey CLT structures. The shaking table test results also evidenced the excellent seismic performance of CLT structures. Pei et al. [11, 12] evaluated the strength reduction factor through performance-based seismic analysis methods. Fragiacomo et al. [13] analyzed the influence of the connection stiffness on the structural seismic response depending on a simplified numerical model of a four-storey CLT structure. Latour and Rizzano [14] evaluated the values of behavior factor for a three-storey CLT building with the traditional hold downs and another CLT building with innovative energy-dissipating connections.

In the previous studies, research results on mechanical properties of CLT connections, lateral performance of CLT wall panels, and dynamic response of CLT structures have been comprehensively reported. However, the inter-storey drift limits for multi-storey CLT structures under various seismic hazard levels, although which are helpful to determine the post-earthquake damage state and judge if a CLT structure has beyond the elastic stage under seismic loads, have not been proposed.

In the performance-based seismic analysis (PBSA) methodology for CLT shear wall structures, the inter-storey drift limits can be provided as the damage measurements to define the post-earthquake damage states of the structural components. In addition, the effective and convenient displacement-based design method has not been developed due to the lack of appropriate inter-storey drift limits for CLT structures. To promote the development of PBSA methodology and displacement-based design method for CLT structures, it is necessary and has a reference meaning for engineering design to conduct an analytical investigation into the inter-storey drift limits of CLT structures. In this paper, a parametric analysis is first carried out on CLT shear walls with various structural configurations using test-calibrated numerical models, and then, three CLT structures are designed as the benchmarks for evaluating the inter-storey drift thresholds under various earthquake hazard levels. Then numerous time-history dynamic analyses are conducted and the curves of cumulative distribution functions (CDFs) which can provide reasonable drift limitations are obtained.

CLT connection and wall modeling

Numerical model for CLT connections

CLT structures consist of CLT shear walls and CLT floor diaphragms. CLT shear walls are connected to the floors using angle brackets (Fig. 1) fastened by screws or nails. To increase the lateral force resisting performance and restrict the rotational movement of the shear wall, hold downs (Fig. 2) are also used to connect the bottom corners of CLT wall to the floor diaphragm. To satisfy the dimension requirements of transportation, CLT panels are usually prefabricated with an appropriate width. During the process of construction, CLT panels are assembled into a shear wall with a larger width along the vertical edge of adjacent panels using screws and nails (i.e., single-surface spline joint, as shown in Fig. 3). In this study, three types of CLT connections that were originally used in the SOFIE project [1] are selected for the benchmark structures, and nonlinear numerical models for the aforementioned CLT connections are developed.

The wall-to-foundation angle bracket used in the test was BMF $90 \times 116 \times 48 \times 3$ mm with eleven 4×60 mm Anker annular ring nails, and the angle bracket was fixed to the foundation with one $\Phi 12$ bolt. The wall-to-floor angle bracket was BMF $100 \times 100 \times 90 \times 3$ mm with eight 4×60 mm Anker annular ring nails, and it was anchored to floor with six 4×60 mm Anker annular ring nails and two additional 4×60 mm HBS screws. WHT540 hold down with twelve 4×60 mm Anker annular ring nails was used for connecting the shear wall to the foundation. WHT440 hold down with nine 4×60 mm Anker annular ring nails was used for connecting the shear

Fig. 1 Angle bracket

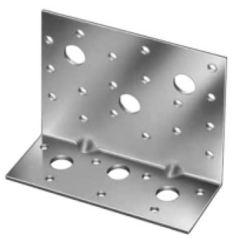

Fig. 2 Hold down

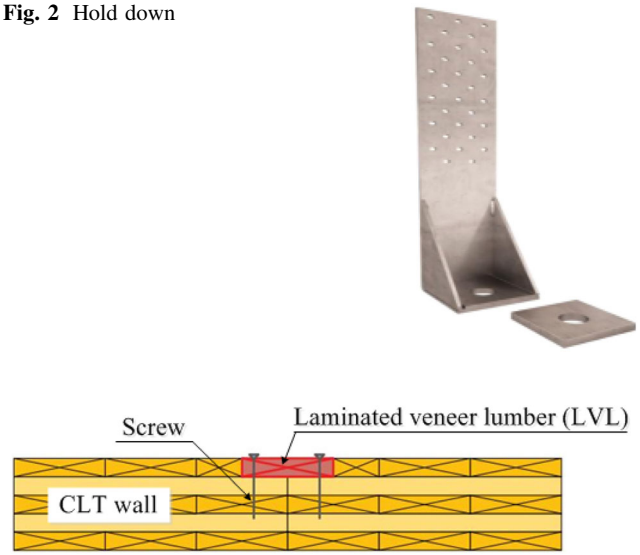

Fig. 3 Single-surface spline joint

wall to the floor diaphragm. Each kind of hold down was anchored to the foundation or floor diaphragm with one Φ16 bolt. For the single-surface spline joint, panel edges were profiled to take a spline of laminated veneer lumber (LVL) strip (Fig. 3). The width and thickness of the LVL strip were 180 mm and 28 mm, respectively. A double row of HBS 8 × 80 mm screws spacing at 150 mm was used for as fasteners of the connection on site. Figure 4 shows all the tested connections in SOFIE project.

Numerical models of the connections were developed using the Pinching4 model [15] in OpenSees [16]. To account for stiffness and strength degradation under cyclic loading, piecewise linear curves that represent a "Pinching" load-deformation response were used in this model. As shown in Fig. 5, 16 parameters (ePd_1, ePf_1, ePd_2, ePf_2, ePd_3, ePf_3, ePd_4, ePf_4, eNd_1, eNf_1, eNd_2, eNf_2, eNd_3, eNf_3, eNd_4, and eNf_4) are used to define the backbone curve. In which, parameters from ePd_1 to ePf_4 are used to define the deformation and force values of the four points on the positive response envelope. Parameters from eNd_1 to eNf_4 are used to define the deformation and force values of the four points on the negative response envelope. Six

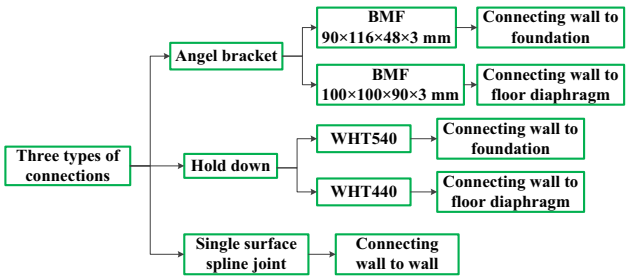

Fig. 4 Three types of CLT connections tested in SOFIE project

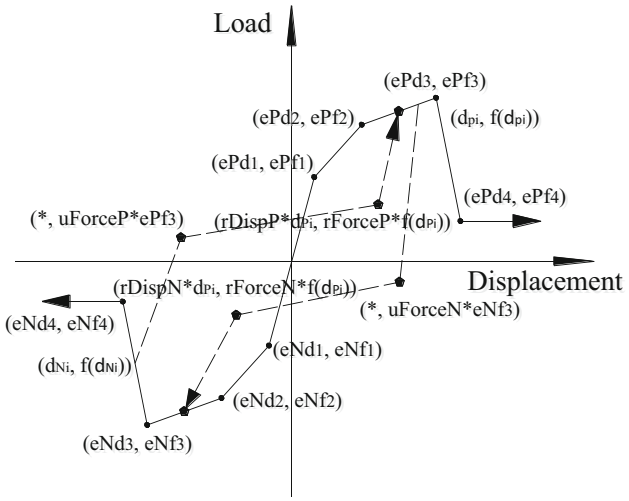

Fig. 5 Pinching4 model

parameters (rDispP, rForceP, uForceP, rDispN, rForceN, and uForceN) are used to define the unload–reload paths and pinching behavior of the CLT connection [17]. In which, parameters of rDispP and rDispN are used to define the ratio of the deformation at which reloading occurs to the maximum and minimum historic deformation demands, respectively. Parameters of rForceP and rForceN are used to define the ratio of the force at which reloading begins to force corresponding to the maximum and minimum historic deformation demands, respectively. Parameters of uForceP and uForceN are used to define the ratio of strength developed upon unloading from negative load to the maximum and minimum strengths developed under monotonic loading, respectively. For the Pinching4 model embedded in the connection model, the damage type was defined as "Energy" to take the damage accumulation of the connection under cyclic load into consideration referring to the general damage index proposed by Park and Ang [18].

Figure 6 shows the schematic of the developed model. The total thickness of the CLT panel is 85 mm, which is

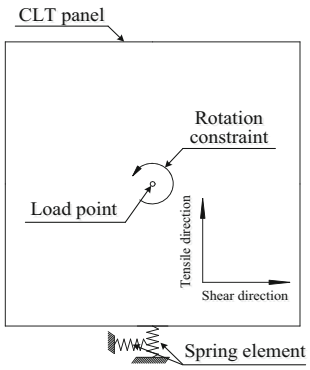

Fig. 6 CLT connection numerical model

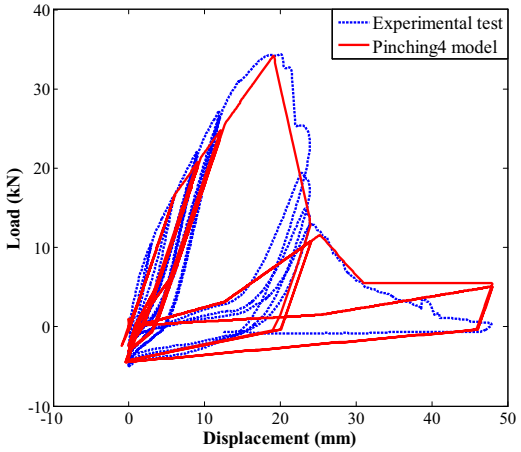

(a) WHT440 loaded longitudinal to the grain

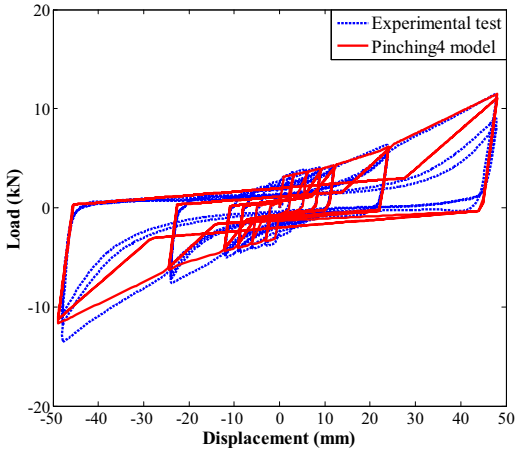

(b) WHT440 loaded perpendicular to the grain

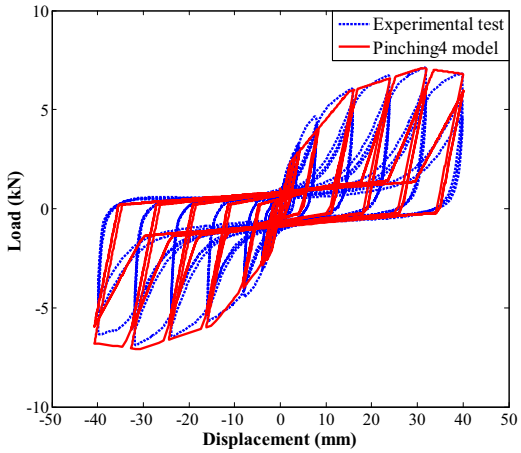

(c) Single surface spline joint loaded longitudinal to the grain

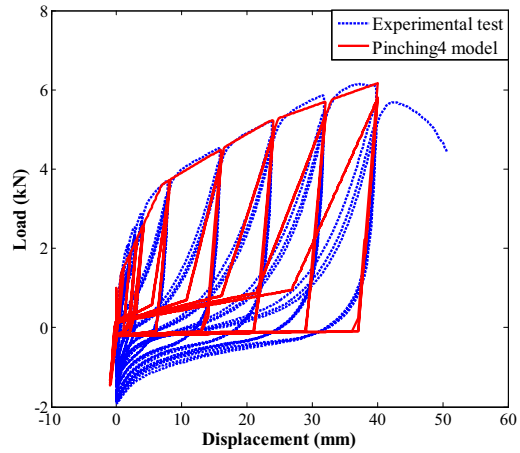

(d) Single surface spline joint loaded perpendicular to the grain

Fig. 7 Hysteretic response of experimental test and Pinching4 model for hold-down WHT440 and single-surface spline joint. **a** WHT440 loaded longitudinal to the grain. **b** WHT440 loaded perpendicular to the grain. **c** Single surface spline joint-loaded longitudinal to the grain. **d** Single surface spline joint-loaded perpendicular to the grain

made up of five orthogonally crossed equal-thickness layers (5 by 17 mm). ShellMITC4 element [19] was used to simulate the CLT panel. According to the results of material property tests, the elastic modulus in the horizontal direction (E_x) and that in the vertical direction (E_y) are 4.6 GPa and 6.7 GPa, respectively. Poisson ratios γ_{xy} and γ_{yx} are 0.19 and 0.27, respectively. The value of shear-through-thickness rigidity G_{xy} is 1.0 GPa. ZeroLength element [20] was used to make the CLT panel connected to the foundation. The aforementioned Pinching4 model was embedded into the ZeroLength element in both the vertical and horizontal directions to simulate the nonlinear mechanical behavior of the connection under combined tensile and shear force. The shear or tensile force was applied on the centre of the panel, where rotational free degree of the panel was fixed. The tests and numerical simulations were both conducted in accordance with the ASTM-CUREE protocol [21].

In this study, the parameters of the Pinching4 model were calibrated by the test results of each kind of CLT connection in both shear and tensile directions. The shear direction and the tensile direction are perpendicular to and parallel to the grain, respectively. The numerical models of the angle bracket hold down and single-surface spline joint were developed, respectively. As examples, the comparisons of hysteretic predictions from both models and test results for hold down WHT440 and single-surface spline joint in perpendicular and longitudinal to the grain are given in Fig. 7. Good agreement can be observed between model predictions and experimental results. It is noted that

Table 1 Calibrated connector parameters for Pinching4 model

Parameters	Angle bracket				Hold down				Single-surface spline joint	
	BMF 90 × 116 × 48 × 3 (mm)		BMF 100 × 100 × 90 × 3 (mm)		WHT540		WHT440			
	Shear	Tension	Shear	Tension	Shear	Tension	Shear	Tension	Shear	Tension
ePf_1 (kN)	4.36	9.81	6.30	5.32	3.94	7.58	3.13	16.30	2.30	1.36
ePf_2 (kN)	20.26	18.38	16.60	12.00	10.20	33.05	4.24	34.26	5.90	3.60
ePf_3 (kN)	27.40	23.13	16.40	4.22	11.70	45.38	5.70	12.88	7.10	5.16
ePf_4 (kN)	19.00	14.46	7.36	3.45	19.60	15.83	10.59	5.448	6.80	5.80
ePd_1 (mm)	2.00	3.58	4.00	2.00	2.00	1.30	0.90	5.80	2.00	0.70
ePd_2 (mm)	13.00	10.00	22.20	6.00	22.50	9.00	11.00	19.10	15.00	7.00
ePd_3 (mm)	29.00	18.00	44.00	41.70	44.00	18.00	22.00	24.00	31.00	23.00
ePd_4 (mm)	40.00	33.00	70.00	50.00	76.00	35.00	44.00	31.00	40.00	34.00
eNf_1 (kN)	−4.36	−9.81	−6.30	−5.32	−3.94	−7.58	−3.13	−16.30	−2.30	−1.36
eNf_2 (kN)	−20.26	−18.38	−16.60	−12.0	−10.20	−33.05	−4.24	−34.26	−5.90	−3.60
eNf_3 (kN)	−27.40	−23.13	−16.40	−4.22	−11.70	−45.38	−5.70	−12.88	−7.10	−5.16
eNf_4 (kN)	−19.00	−14.46	−7.36	−3.45	−19.60	−15.83	−10.59	−5.45	−6.80	−5.80
eNd_1 (mm)	−2.00	−3.58	−4.00	−2.00	−2.00	−1.30	−0.90	−5.80	−2.00	−0.70
eNd_2 (mm)	−13.00	−10.00	−22.20	−6.00	−22.50	−9.00	−11.00	−19.10	−15.00	−7.00
eNd_3 (mm)	−29.00	−18.00	−44.00	−41.70	−44.00	−18.00	−22.00	−24.00	−31.00	−23.00
eNd_4 (mm)	−40.00	−33.00	−70.00	−50.00	−76.00	−35.00	−44.00	−31.00	−40.00	−34.00
rDispP	0.60	0.72	0.55	0.65	0.45	0.7	0.55	0.5	0.70	0.65
rForceP	0.25	0.18	0.30	0.31	0.25	0.15	0.25	0.27	0.20	0.15
uForceP	0.05	0.02	0.03	0.23	0.01	0.03	0.03	0.03	0.03	0.02
rDispN	0.60	0.72	0.55	0.65	0.45	0.7	0.55	0.5	0.70	0.65
rForceN	0.25	0.18	0.30	0.31	0.25	0.15	0.25	0.27	0.20	0.15
uForceN	0.05	0.02	0.03	0.23	0.01	0.03	0.03	0.03	0.03	0.02
gD1	0.90	0.97	0.90	0.97	0.90	0.97	0.90	0.97	0.90	0.97
gD2	0	0	0	0	0	0	0	0	0	0
gD3	0	0	0	0	0	0	0	0	0	0
gD4	0	0	0	0	0	0	0	0	0	0
gDLim	0.05	0.05	0.05	0.05	0.05	0.05	0.05	0.05	0.05	0.03

in Fig. 7b, the stiffness in the experimental test is slightly larger than that in the model in the negative side of the hysteretic curves. This is because in the experimental test, the shear force was loaded and unloaded in the positive direction initially and then in the negative direction subsequently, and the shear force applied in the negative direction had to overcome the residual deformation caused by the force applied in the positive direction. As a result, a larger stiffness was observed on the negative loading cycles of the hysteretic curves. In contrast, the stiffness on both sides of the numerical hysteretic curves was identical due to the balanced parameters defined in Pinching4 model. The calibrated parameters of Pinching4 model for the three typical types of connections are listed in Table 1.

Numerical model for CLT shear walls

Under lateral cyclic loading, the movement of a CLT shear wall can be decomposed into two directions: the first is the sliding movement between the bottom of the panel and the foundation or floor diaphragm and the second is the uplift at the bottom corner of the wall. For CLT shear wall modeling, angle bracket or hold down between the wall panel and the foundation was simplified as two coupling orthogonal springs, as shown in Fig. 8. The Pinching4 model was embedded into the coupling springs to simulate the mechanical behavior of the angle bracket and hold down connections. For a double-panel wall connected through single-surface spline joint, similar work was done to simulate the mechanical behavior of the spline joint

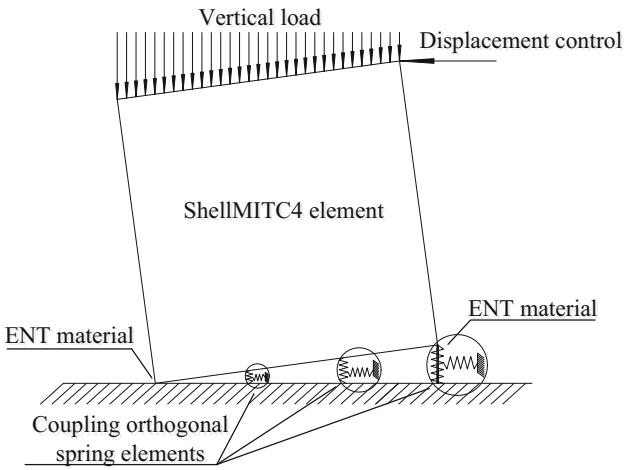

Fig. 8 Numerical model of CLT shear wall

between the two adjacent panels. To simulate the compressive stiffness of the contact surface between the wall bottom and the foundation, the elastic-no tension (ENT) material, which only provides a compressive stiffness, was utilized as vertical spring elements. Since it was shown from SOFIE project that the friction between the wall and the foundation had little influence on the mechanical properties of the CLT walls, friction effect between the wall and the foundation was also ignored in this model.

The compressive stiffness of the ENT material in the model was calibrated with a series of CLT shear wall tests carried out by Gavric et al. [22]. The calibration was an iterative process. Trial compressive stiffness was first used in a numerical wall model, and the loading protocol applied on the model was the same as that used in the test. Numerical predictions of hysteresis curves were compared to the test results. The trial compressive stiffness was then adjusted until a good match was obtained. It is noted from Fig. 9 that the simulated response is quite close to the test once the compressive stiffness of ENT material is properly calibrated. It is worth mentioning that the values of compressive stiffness are in the range of 1500–2000 N/mm^2.

Parametric analysis of CLT shear walls

Deformation mode

Four possible deformation components exist for a single-panel CLT shear wall, as illustrated in Fig. 10: (1) rocking, (2) sliding, (3) shear, and (4) bending [23]. Table 2 presents the contributions of the four deformation components to the total lateral deformation for three single-panel CLT shear walls with identical geometric dimensions (i.e., 2950 mm in length and 2950 mm in height). It is noted that for wall No. 1, the contribution of sliding deformation accounts for a larger percentage compared to those of wall No. 2 and wall No. 3, and this is due to fewer angle brackets were used to connect wall No. 1 to the foundation. Rocking deformation contribution of wall No. 2 accounts for a smaller percentage compared to that of wall No. 3. This is due to wall No. 3 has the smallest gravity load, which can provide effective constraint for rocking deformation. In addition, it turns out that in-plane bending and

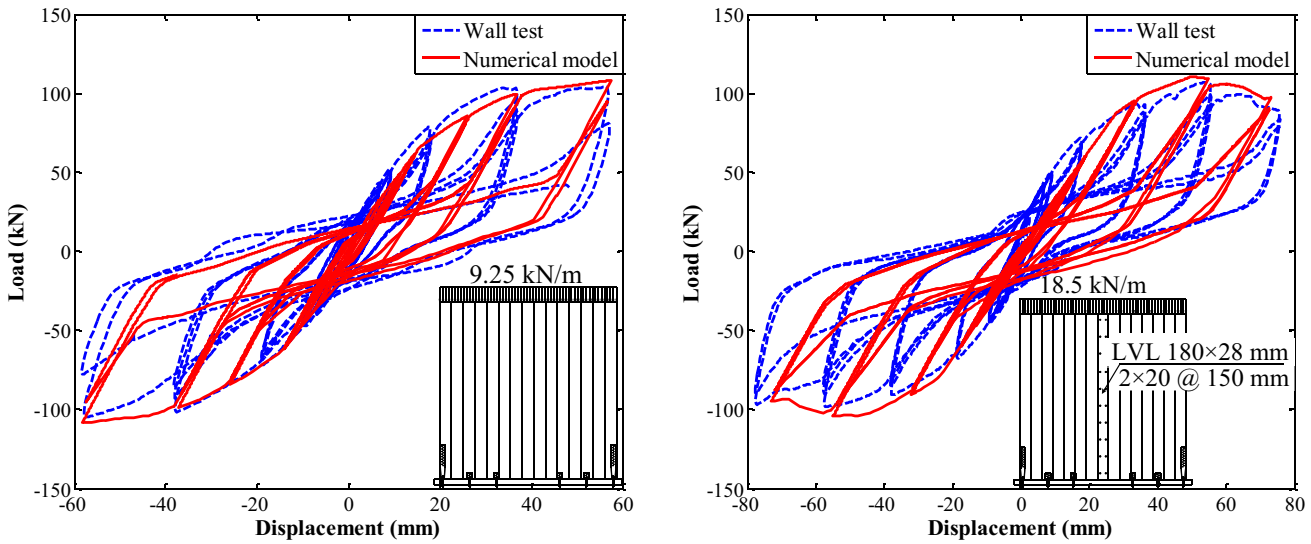

(a) Single-panel CLT wall

(b) Double-panel CLT wall connected by spline joint

Fig. 9 Comparison of tested and analytically predicted wall response with calibrated compressive stiffness. **a** Single-panel CLT wall. **b** Double-panel CLT wall connected by spline joint

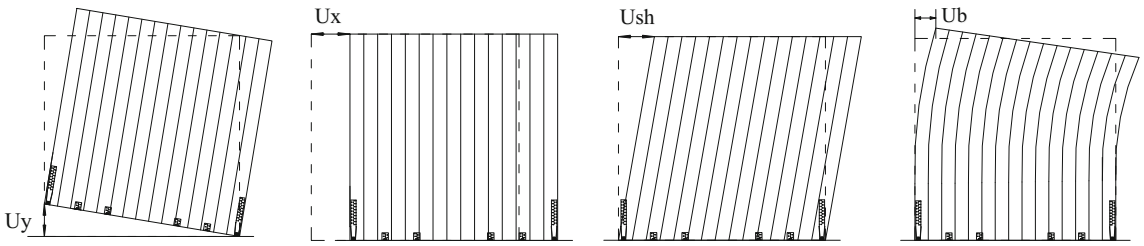

Fig. 10 Deformation modes of a single-panel CLT wall. **a** Rocking. **b** Sliding. **c** Shear. **d** Bending

Table 2 Contributions of deformation components for the three single-panel CLT shear walls

Wall number	Gravity	Connections	Data resource	Rocking	Sliding	Shear and bending	Main deformation mode
1	18.5 kN/m	2 angle brackets; 2 hold downs	Test	24.3%	73.0%	2.7%	Sliding
			Model	4.0 mm	13.9 mm	1.6 mm	Sliding
				20.4%	71.4%	8.3%	
2	18.5 kN/m	4 angle brackets; 2 hold downs	Test	42.1%	55.9%	2.0%	Sliding-rocking
			Model	9.0 mm	13.3 mm	1.7 mm	Sliding-rocking
				37.3%	55.5%	7.2%	
3	9.25 kN/m	4 angle brackets; 2 hold downs	Test	56.8%	41.2%	2.0%	Rocking-sliding
			Model	10.0 mm	7.6 mm	1.7 mm	Rocking-sliding
				52.1%	39.3%	8.6%	

CLT cross-laminated timber

shear deformation can almost be negligible due to the large in-plane stiffness of CLT panels.

Gravity load

In this section, parametric studies were conducted to research the influence of gravity load on the lateral behavior of CLT shear walls. The hysteretic curves of aforementioned CLT walls are shown in Fig. 11. Equivalent energy elastic–plastic (EEEP) method provided in ASTM E2126 [21] was used to translate the irregular backbone curves of the hysteretic curves into ideally linear elastic–plastic curves. The ultimate force ($F_{\max}$), yielding force (F_y) and related displacement (Δ_y), ultimate displacement (Δ_U), elastic displacement (Δ_E), elastic lateral stiffness (K_e), and ductility ratio (D_r) of the walls can be determined and compared as listed in Table 3. Results show that for single-panel walls, an increment of 9.25 kN/m of the gravity load leads to a 10–15% increase in the ultimate force, yielding force, and ductility ratio. For couple-panel walls, the increase of gravity load from 0 kN/m to 18.5 kN/m leads to a slight increase in ultimate force, elastic displacement, yielding force, and ductility ratio. However, the increase of gravity load from 18.5 kN/m to 27.0 kN/m leads to a significant decrease in ultimate force, yielding force and ductility ratio, which is caused by the shear failure and the occurrence of large relative movement in the spline joint between adjacent panels.

Screw spacing on spline joint

Further parametric studies were also conducted to research the influence of spline joint configuration on the lateral behavior of double-panel CLT walls. Four values of screw spacing in the single-surface spline joint (i.e., 75, 150, 300, and 400 mm) were considered in the numerical wall model. Identical gravity load of 18.5 kN/m was considered for all the double-panel CLT walls. The hysteretic curves of the double-panel CLT walls with different screw spacing are shown in Fig. 12, and Table 4 gives the mechanical properties of double-panel CLT walls. It is shown that the decrease of screw spacing from 400 mm to 150 mm leads to a significant increase in elastic lateral stiffness, yielding force, and ultimate force, but it leads to a slight decrease in ductility ratio. Interestingly, when the spacing decreased from 150 mm to 75 mm, the ultimate force and elastic lateral stiffness of the wall cease to increase.

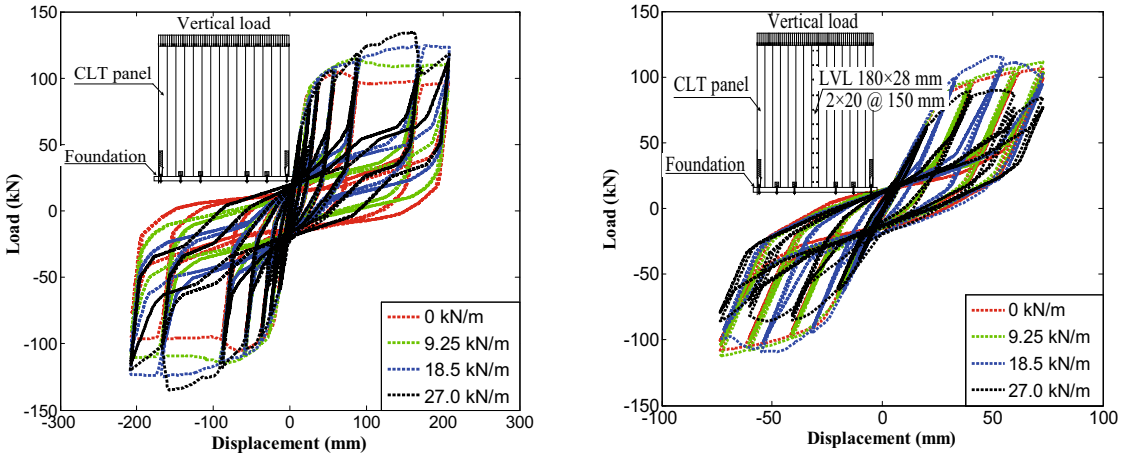

(a) Single-panel wall **(b)** Double-panel wall with spline joint

Fig. 11 Influence of gravity load on the behavior of CLT walls. **a** Single-panel wall. **b** Double-panel wall with spline joint

Table 3 Mechanical parameters of CLT shear walls

Wall configuration	Gravity	0 kN/m	9.25 kN/m	18.5 kN/m	27.0 kN/m
Single-panel CLT wall	F_{max}	102.50 kN	114.51 kN	124.74 kN	142.32 kN
	Δ_E	10.41 mm	11.35 mm	7.90 mm	8.92 mm
	K_e	3.93 kN/mm	4.04 kN/mm	6.32 kN/mm	6.38 kN/mm
	Δ_U	165.6 mm	153.42 mm	165.02 mm	220.12 mm
	F_y	87.46 kN	104.05 kN	114.06 kN	126.60 kN
	Δ_y	36.85 mm	29.32 mm	31.15 mm	35.62 mm
	D_r	4.49	5.23	5.30	6.18
Double-panel CLT wall with spline joint spaced at 150 mm	F_{max}	106.37 kN	109.20 kN	112.29 kN	90.12 kN
	Δ_E	12.43 mm	12.66 mm	13.05 mm	10.05 mm
	K_e	3.40 kN/mm	3.45 kN/mm	3.44 kN/mm	3.59 kN/mm
	Δ_U	80.01 mm	85.72 mm	88.23 mm	76.00 mm
	F_y	97.50 kN	98.93 kN	99.21 kN	86.01 kN
	Δ_y	28.65 mm	26.65 mm	19.56 mm	26.49 mm
	D_r	2.79	3.22	4.51	2.86

CLT cross-laminated timber

Design chart for CLT shear walls

The lateral load-resisting parameters for the CLT walls with given geometric configurations were obtained through numerical modeling. The double-panel wall consisted of two panels that were connected using a continuous single-surface spline joint and a double row of HBS 8 × 80 mm screws spacing at 150 mm or 300 mm. The three-panel wall consisted of three panels that were connected to each other using two continuous single-surface spline joints, and a double row of HBS 8 × 80 mm screws spacing at 150 mm or 300 mm was used as fasteners for each spline joint. In each configuration, there were two hold downs and a certain number of angle brackets. To illustrate the configurations, the sketches of a double-panel wall and a three-panel wall are shown in Fig. 13a, b, respectively.

Nonlinear pushover analyses were conducted to obtain the load-resisting properties of a group of CLT shear walls with 32 different configurations. The backbone curves were obtained to identify the ultimate resistance of the walls. Then, the design strength values for the walls were determined by dividing the ultimate strength from the CLT wall backbone curve by a strength safety factor (γ_{od}) of 2.5, which is identical as the one used in the study conducted by Pei et al. [11]. For the CLT wall models connected to the foundation, the gravity from dead load of upper storey was set as 18.5 kN/m. For the CLT wall models connected to the floor diaphragm, the gravity from dead load of upper

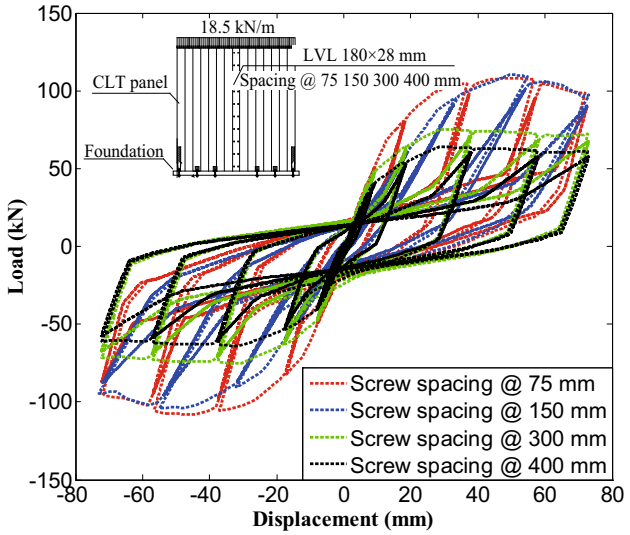

Fig. 12 Influence of spline joint density on mechanical properties of double-panel CLT walls

storey was set as 9.25 kN/m. Tables 5 and 6 provide the design lateral capacities of CLT shear walls with various configurations. It shows that the CLT walls with added angle brackets will have a significant increase in design lateral capacity. For some CLT wall configurations, the lateral load-resisting capacity ceases to increase when the spacing of the fasteners is decreased from 300 mm to 150 mm. It is because that the fastener spacing of 300 mm in the spline joint has been enough to ensure reliable force transfer between adjacent panels.

Modeling of CLT shear wall structure

Selection of seismic design parameters

In this study, three CLT shear wall structures (i.e., 3-storey, 6-storey, and 9-storey) were designed using the equivalent static force procedure (ESFP) given in NBCC [24]. The seismic reduction factor (R_d) and the over-strength factor (R_0) have to be known for generating the seismic demand on the buildings. According to the study conducted by Ceccotti et al. [10] and Ceccotti and Sandhaas [25] in SOFIE project, the value of R_d was chosen to be 3.0. The thickness and the mechanical properties of the CLT panels in SOFIE project were the same as that we use in the numerical model. Therefore, the R_d value of 3.0 was more appropriate to be used in the study. The value of R_0 was

Table 4 Mechanical properties of double-panel CLT shear walls with different screw spacing

Screw spacing	75 mm	150 mm	300 mm	400 mm
F_{max}	110.29 kN	110.21 kN	80.18 kN	64.14 kN
Δ_E	6.83 mm	7.01 mm	9.95 mm	10.25 mm
K_e	6.48 kN/mm	6.32 kN/mm	3.22 kN/mm	2.51 kN/mm
Δ_U	88.97 mm	83.23 mm	97.29 mm	100.47 mm
F_y	98.45 kN	95.34 kN	75.78 kN	73.42 kN
Δ_y	17.13 mm	15.10 mm	15.06 mm	14.56 mm
D_r	5.19	5.51	6.46	6.90

CLT cross-laminated timber

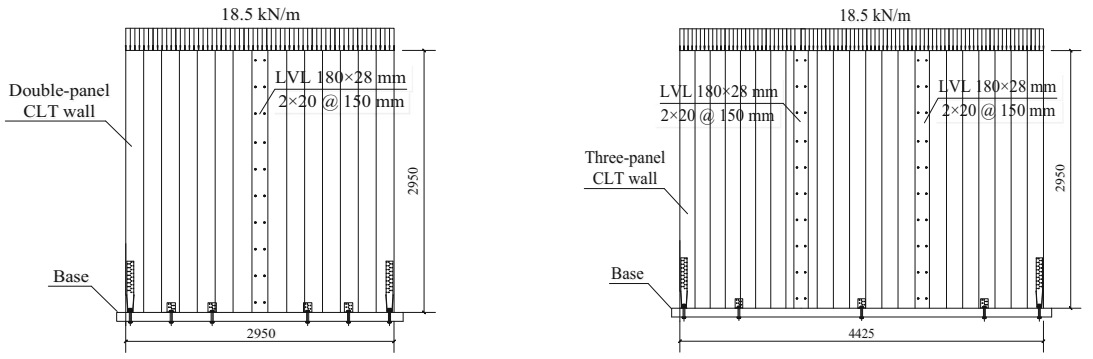

(a) Double-panel wall with 2 hold downs and 4 angle brackets

(b) Three-panel wall with 2 hold downs and 3 angle brackets

Fig. 13 Sketches of CLT shear walls (except indicated, all dimensions are in mm). **a** Double-panel wall with 2 hold downs and 4 angle brackets. **b** Three-panel wall with 2 hold downs and 3 angle brackets

Table 5 Design lateral capacity table for CLT walls (connected to foundation)

Length of CLT shear wall	1475 mm		2950 mm		4425 mm		5900 mm	
Number of angle brackets	1	2	2	4	3	6	4	8
Single-panel wall	11.58 kN	12.43 kN	30.00 kN	49.89 kN				
Double-panel wall with spline joint @ 150 mm				44.12 kN	33.08 kN	69.59 kN	49.01 kN	92.12 kN
Double-panel wall with spline joint @ 300 mm				33.31 kN	32.93 kN	52.76 kN	43.05 kN	57.26 kN
Three-panel wall with spline joint @ 150 mm					32.98 kN			
Three-panel wall with spline joint @ 300 mm					32.64 kN			

CLT cross-laminated timber

Table 6 Design lateral capacity table for CLT walls (connected to floor)

Length of CLT shear wall	1475 mm		2950 mm		4425 mm		5900 mm	
Number of angle brackets	1	2	2	4	3	6	4	8
Single-panel wall	7.90 kN	8.55 kN	20.46 kN	26.28 kN				
Double-panel wall with spline joint @ 150 mm				26.05 kN	22.67 kN	39.68 kN	33.19 kN	54.99 kN
Double-panel wall with spline joint @ 300 mm				25.11 kN	22.35 kN	38.82 kN	33.04 kN	46.64 kN
Three-panel wall with spline joint @ 150 mm					19.80 kN			
Three-panel wall with spline joint @ 300 mm					19.76 kN			

CLT cross-laminated timber

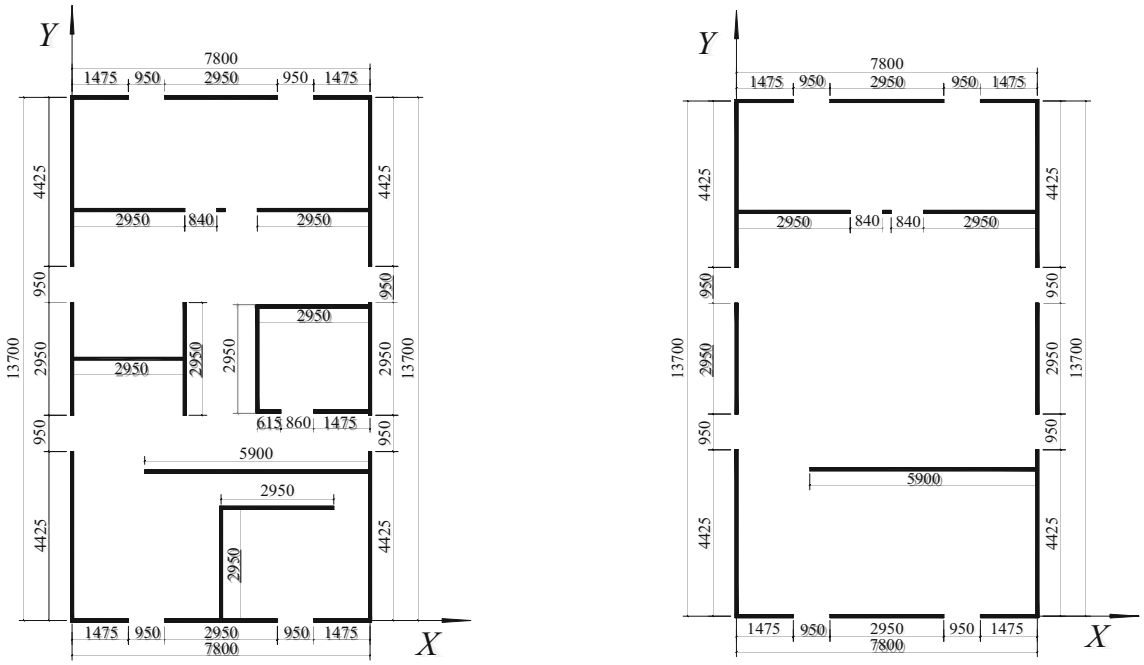

(a) Floor plan (Storey 1-5) **(b)** Floor plan (Storey 6)

Fig. 14 Floor plan of the 6-storey building (all dimensions are in mm). **a** Floor plan (Storey 1–5). **b** Floor plan (Storey 6)

chosen to be 1.5. The building important factor (I_E) was set as 1.0. The fundamental periods of the 3-storey, 6-storey, and 9-storey CLT buildings determined using formula provided by *ASCE/SEI 7-10* [26] were 0.269 s, 0.437 s, and 0.592 s, respectively. The design hazard level of the seismic response spectrum in NBCC corresponds to a

Table 7 Shear wall selection for the 6-storey CLT building (*X*-direction)

Length	1475 mm			2950 mm			5900 mm		
Storey	Number of walls	Configuration	Capacity	Number of walls	Configuration	Capacity	Number of walls	Configuration	Capacity
1	5	Single-panel wall; 2 angle brackets; 2 hold downs;	12.43 kN	7	Single-panel wall; 2 angle brackets; 2 hold downs;	29.99 kN	1	Double-panel wall with spline joint @ 150 mm; 8 angle brackets; 2 hold downs;	92.12 kN
2	5	Single-panel wall; 2 angle brackets; 2 hold downs;	8.55 kN	7	Single-panel wall; 4 angle brackets; 2 hold downs;	26.28 kN	1	Double-panel wall with spline joint @ 150 mm; 8 angle brackets; 2 hold downs;	54.99 kN
3	5	Single-panel wall; 2 angle brackets; 2 hold downs;	8.55 kN	7	Double-panel wall with spline joint @ 300 mm; 4 angle brackets; 2 hold downs;	25.11 kN	1	Double-panel wall with spline joint @ 150 mm; 8 angle brackets; 2 hold downs;	54.99 kN
4	5	Single-panel wall; 2 angle brackets; 2 hold downs;	8.55 kN	7	Single-panel wall; 2 angle brackets; 2 hold downs;	20.46 kN	1	Double-panel wall with spline joint @ 300 mm; 4 angle brackets; 2 hold downs;	33.04 kN
5	5	Single-panel wall; 2 angle brackets; 2 hold downs;	8.55 kN	7	Single-panel wall; 2 angle brackets; 2 hold downs;	20.46 kN	1	Double-panel wall with spline joint @ 300 mm; 4 angle brackets; 2 hold downs;	33.04 kN
6	4	Single-panel wall; 2 angle brackets; 2 hold downs;	8.55 kN	4	Single-panel wall; 2 angle brackets; 2 hold downs;	20.46 kN	1	Double-panel wall with spline joint@300 mm; 4 angle brackets; 2 hold downs;	33.04 kN

CLT cross-laminated timber

Table 8 Shear wall selection for the 6-storey CLT building (*Y*-direction)

Length	2950 mm			4425 mm		
Storey	Number of walls	Configuration	Capacity	Number of walls	Configuration	Capacity
1	5	Single-panel wall; 2 angle brackets; 2 hold downs;	29.99 kN	4	Double-panel wall with spline joint@300 mm; 6 angle brackets; 2 hold downs;	52.76 kN
2	5	Single-panel wall; 4 angle brackets; 2 hold downs;	26.28 kN	4	Double-panel wall with spline joint@150 mm; 6 angle brackets; 2 hold downs;	39.68 kN
3	5	Single-panel wall; 2 angle brackets; 2 hold downs;	20.46 kN	4	Double-panel wall with spline joint@150 mm; 6 angle brackets; 2 hold downs;	39.68 kN
4	5	Single-panel wall; 2 angle brackets; 2 hold downs;	20.46 kN	4	Double-panel wall with spline joint@300 mm; 6 angle brackets; 2 hold downs;	38.82 kN
5	5	Single-panel wall; 2 angle brackets; 2 hold downs;	20.46 kN	4	Three-panel wall with spline joint@300 mm; 3 angle brackets; 2 hold downs;	19.76 kN
6	2	Single-panel wall; 2 angle brackets; 2 hold downs;	20.46 kN	4	Three-panel wall with spline joint@300 mm; 3 angle brackets; 2 hold downs;	19.76 kN

CLT cross-laminated timber

probability of exceedance of 2% in 50 years. Because the seismic response spectrum for rare seismic hazard level in Chinese code *GB50011-2010* [27] also corresponds to the same probability of exceedance for the same span of time, it was used as the design seismic response spectrum in this study. It was assumed that the buildings were located in Shanghai China, which corresponds to the maximum acceleration of 0.95 g in the design seismic response spectrum. The periods of the upper and lower limit for the plateau region of the spectrum are 0.45 s and 0.1 s, respectively.

Shear wall selection

After the seismic design parameters have been determined, the shear demand in each storey of the building can be calculated following ESFP. Taking the 6-storey CLT building as an example, the seismic weight for each storey of the building was 305.1 kN, except that it was 223.7 kN for the roof level. The theoretical fundamental period (T_1) was 0.437 s. The elastic spectral acceleration at fundamental period [Sa (T_1)] was 0.95 g. Then, the base shear demand was determined as 1396.2 kN. The distribution of the equivalent lateral force over the height of the building and the shear demand for each individual storey in the 6-storey CLT building were obtained. The design lateral capacity tables (i.e., Tables 5 and 6) were further used to select the CLT wall configurations with adequate resistance to satisfy the storey shear demands utilizing R_0 and R_d. The wall selection was conducted, so that the total wall resistance was larger than the shear demand for every individual storey and in each direction of the building. The floor layout for the 6-storey building is shown in Fig. 14. Based on the floor plan of each storey and the design chart for CLT shear walls, the shear wall selection for each individual storey was conducted. Tables 7 and 8 show the results of the shear wall selection for the 6-storey building in *X*-direction and *Y*-direction, respectively. The procedures of shear demand calculation and shear wall selection for the 3-storey and 9-storey CLT buildings were similar to that for the 6-storey building.

Simplified numerical model of CLT structure

Since hundreds of CLT shear walls and thousands of connections are incorporated in a multi-storey building, it is complicated and impossible to develop a meticulous structural model in OpenSees. In this study, a simplified structural model was developed to simulate the seismic performance of a multi-storey building under seismic loads. Simplified shear wall model (Fig. 15) was utilized to develop the simplified structural model. The lateral performance of each CLT wall can be simulated using a twoNodeLink element [28]. The twoNodeLink element is defined by two nodes with different coordinates and has 1–6 degrees of freedoms, making it an appropriate element

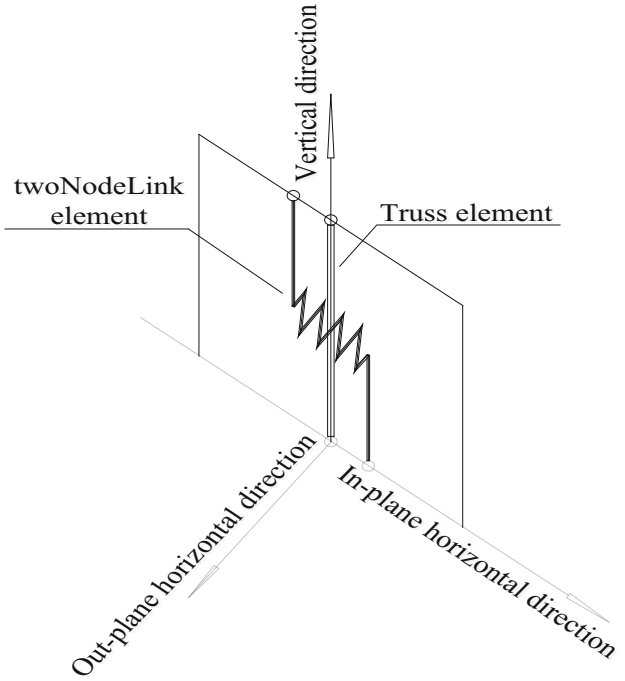

Fig. 15 Simplified shear wall model

to simulate the lateral performance of shear wall. In addition, a Truss element was added into the wall model to provide the compressive stiffness of the shear wall under vertical load. The size of the cross section of the Truss element was the same as that of the shear wall. The calibrated Pinching4 model was embedded into the twoNodeLink element to simulate the in-plane lateral performance of CLT shear wall.

Figure 16 shows the kinematic assumptions of the simplified structural model in OpenSees. Each shear wall model incorporated in the simplified structural model consists of one twoNodeLink and one Truss element. The wall model placed in *X*-direction and *Y*-direction can deformed as the adjacent diaphragms (diaphragm *i* and *j*) move relative to each other, generating lateral resisting

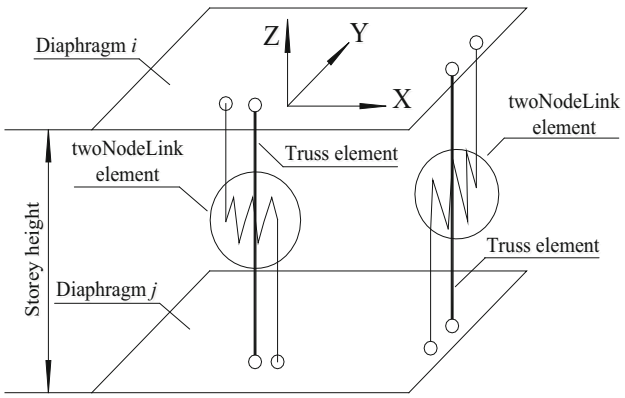

Fig. 16 Kinematic assumptions of the simplified structural model

forces and providing inter-storey stiffness. Because of the high in-plane stiffness for CLT panels, the floor diaphragms are assumed to be rigid plates and are connected using twoNodeLink and Truss elements.

Based on the simplified numerical models of the 3-storey, 6-storey, and 9-storey CLT buildings, the natural periods were also calculated. The natural periods of the 3-storey, 6-storey, and 9-storey buildings from the numerical models were 0.445 s, 0.770 s and 0.875 s, respectively. These natural periods were larger than the code formulation estimations, which were 0.269 s, 0.437 s and 0.592 s for 3-storey, 6-storey, and 9-storey buildings. This was due to the formula for estimating structural periods from *ASCE/SEI 7-10* [26] can be applied to all non-concrete shear wall structures. Since the lateral stiffness of CLT shear wall is normally less than that of other types of shear walls, larger natural periods from models were obtained for the buildings. In addition, since only the structural components were considered in the models, ignoring the stiffness contribution from non-structural components in the models can also lead to larger natural periods. Similar trend between natural and formula-based periods was reported by Pei et al. [11, 12].

Numerical simulation of multi-storey CLT buildings

Ground motions

A suite of 41 biaxial earthquake ground motions representing pulse-type (near-field) motions were used in the study. The pulse-type (near-field) motions represent ground shakings relatively closer to fault rupture during some larger earthquakes and they satisfy the motions requirements of the site condition of Shanghai defined in Chinese code *GB50011-2010* [27]. The ground motions were scaled to three groups of motions corresponding to frequent, medium, and rare seismic ground motions, respectively. The response spectra accelerations of the scaled motions should match the design response spectrum representing each of the three hazard levels between the natural and formula-based periods of a CLT building. Because there were two components from each motion record, the spectrum of the stronger motion component was scaled to the design response spectrum, while the other component was scaled with the same scale factor, so that the ratio between the two components was the same as that of the un-scaled motion. Figure 17 shows the response spectrums of the stronger ground motions components and their comparison with the Shanghai design response spectrums in different seismic hazard levels for the 6-storey building. The response spectrums and comparison for the 3-storey and 9-storey CLT buildings are nearly the same as that for the

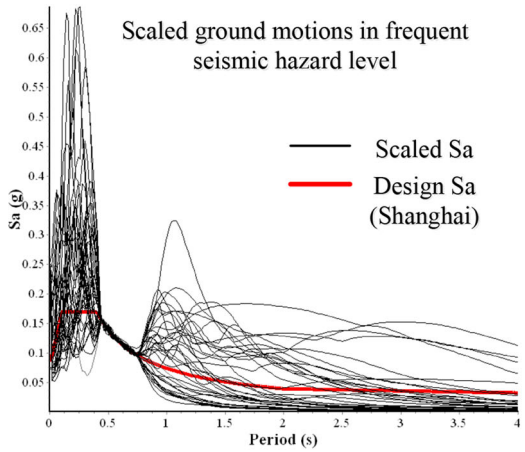

(a) Frequent seismic hazard level

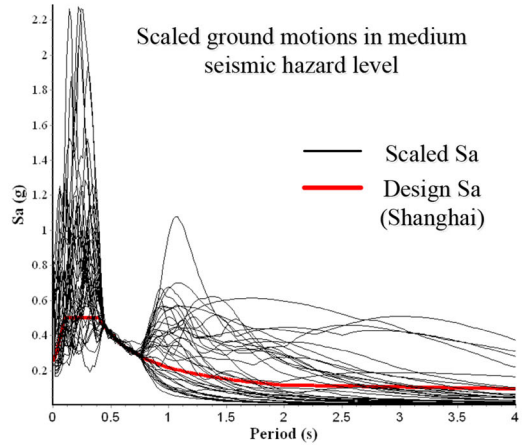

(b) Medium seismic hazard level

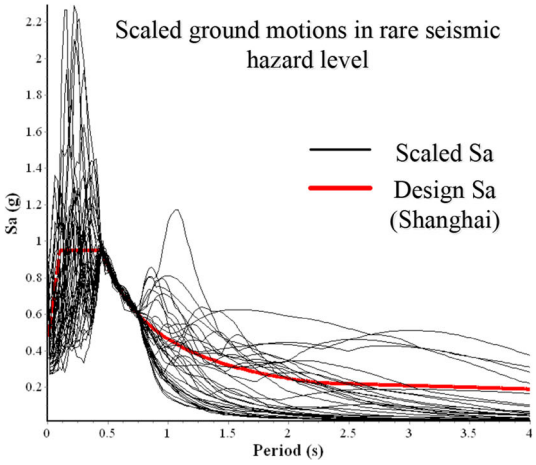

(c) Rare seismic hazard level

Fig. 17 Response spectrums and their comparison with the Shanghai design spectrums for the 6-storey CLT building (Sa: seismic acceleration). **a** Frequent seismic hazard level. **b** Medium seismic hazard level. **c** Rare seismic hazard level

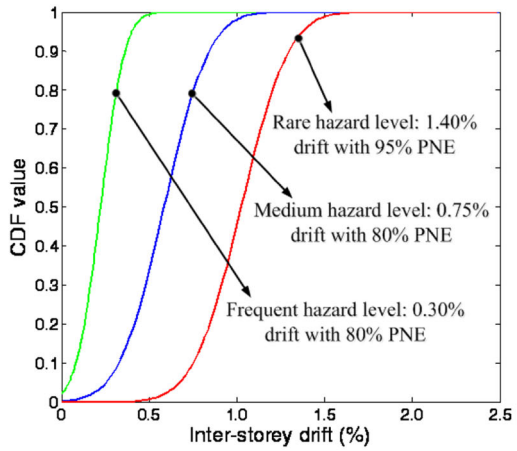

(a) 3-storey CLT building

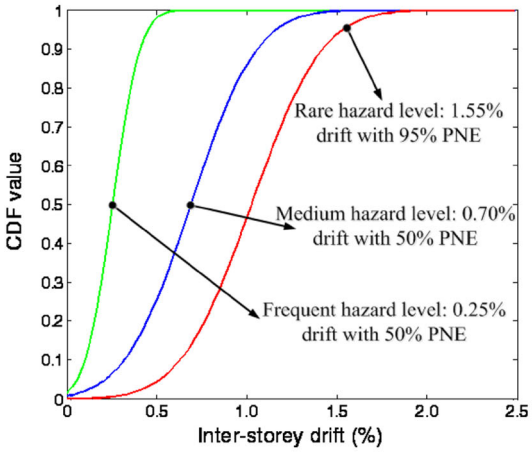

(b) 6-storey CLT building

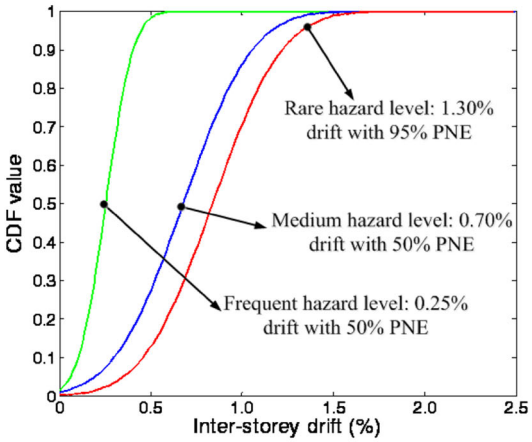

(c) 9-storey CLT building

Fig. 18 CDFs of the maximum inter-storey drifts. **a** 3-storey CLT building. **b** 6-storey CLT building. **c** 9-storey CLT building

Table 9 Limit inter-storey drifts under different hazard levels

CLT buildings	Three hazard levels		
	Frequent (%)	Medium (%)	Rare (%)
3-storey	0.30	0.75	1.40
6-storey	0.25	0.70	1.55
9-storey	0.25	0.70	1.30

CLT cross-laminated timber

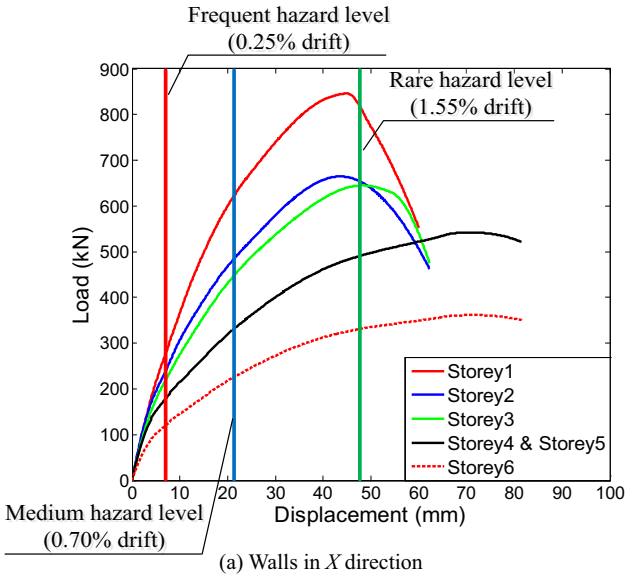

(a) Walls in *X* direction

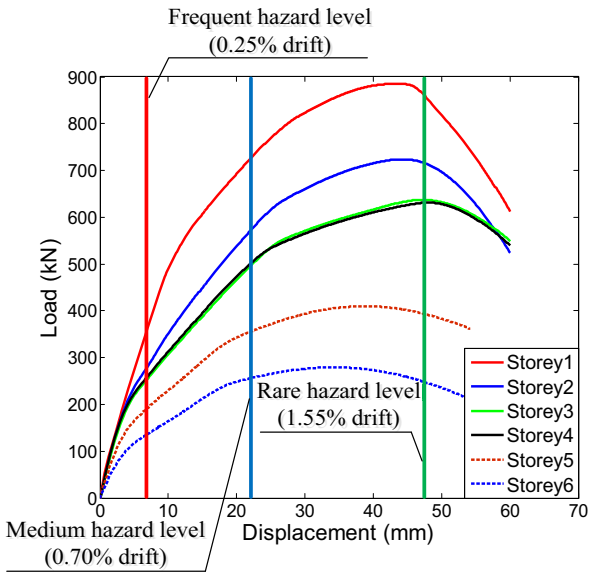

(b) Walls in *Y* direction

Fig. 19 Backbone curves of the 6-storey building versus the target lines of the three hazard levels. **a** Walls in *X*-direction, **b** Walls in *Y*-direction

6-storey building except the natural and formula-based periods of the buildings are different.

Inter-storey drift limitations under different hazard levels

The 41 biaxial near-field ground motions scaled to three target seismic hazard levels were used as the seismic hazard input for the time-history dynamic analysis. Each of biaxial ground motions was then rotated by 90° and also used as the seismic hazard input. So each of the three buildings was analyzed for a total of 82 earthquakes at each hazard level. During the time-history analysis, the maximum inter-storey drift experienced by the structure at any storey and in each direction was recorded. Because a total of two inter-storey drifts in *X*-direction and *Y*-direction were recorded at each time step, the value of the adopted inter-storey drift in the study was the square root of the two inter-storey drifts recorded. With 82 maximum drift values for each seismic hazard level, these maximum drift values were rank-ordered and empirical CDFs were used to plot the CDFs curves. The CDFs curves of the maximum inter-storey drifts for each building are shown in Fig. 18.

Based on the distributions of maximum inter-storey drifts, one can select the appropriate drift limitations under different hazard levels for seismic design given a probability of non-exceedance (PNE) for each hazard level. The PNE value for each of the three buildings in rare seismic hazard level was set to be 95% according to the Chinese code *GB50068-2008* [29]. For the 3-storey building, the value of PNEs in frequent and medium seismic hazard levels was set as 80%, which was the same as that adopted in the study conducted by Pei et al. [11]. For the 6-storey and 9-storey buildings, the value of PNEs in frequent and medium seismic hazard levels was set to be 50%. Considering the seismic design for the 6-storey and 9-storey buildings should be more conservative than that for the 3-storey building, the PNE for the 6-storey and 9-storey buildings (50%) is smaller than that for the 3-storey building (80%). A smaller PNE value will result in a smaller drift limitation, and it will provide a more conservative controlled target for the displacement-based seismic design procedure. The inter-storey drift limitations under the three hazard levels for the benchmarks building are listed in Table 9.

To verify the obtained drift limitation values, the drift limitations for the 6-storey building were discussed as an example. The backbone curves of the shear walls in each storey of the 6-storey building were superimposed. Figure 19 shows the backbone curves of the 6-storey building versus the drift target lines of the three hazard levels. It is noted that the drift limitation of the frequent hazard level approximately represents the upper limit of the elastic stage for the structure. The drift limitation of the medium hazard level is used to judge if the post-earthquake structure can be restored. If the maximum

inter-storey drift recorded is larger than the drift limitation of the medium hazard level, extensive plastic deformation is expected with in most of the structural members. The drift limitation of the rare hazard level is used as an alerted threshold value to make sure that the structure would not collapse even under rare hazard level earthquakes. As is shown in Fig. 19, the displacement corresponding to the target line of rare hazard level is just beyond the ultimate capacity of the shear walls, which indicates that the building still has a portion of the load-resisting capability against collapse.

Conclusions

This paper presents an investigation to quantify the seismic performance of CLT shear walls and multi-storey CLT structures. Parametric analyses revealed that the angle brackets were very effective on constraining the sliding deformation of the shear walls, while the applied gravity load could effectively control the rocking deformation of the shear walls. Furthermore, for the magnitude of the applied gravity loads, the single-panel wall with larger gravity loads tends to have higher ultimate force, yielding force, and ductility ratio. However, the double-panel wall with a larger gravity loads tends to have smaller ultimate force, yielding force, and ductility ratio due to the shear failure in the spline joint. Based on time-history dynamic analyses, it is recommended that for low-rise CLT building within three stories, values of 0.30%, 0.75%, and 1.40% can be considered as the drift limitations for frequent, medium, and rare seismic hazard levels, respectively. For 6-storey and 9-storey buildings, 0.25%, 0.70%, and 1.30% can be considered as drift limitations for frequent, medium, and rare seismic hazard levels, respectively. The drift limitations obtained in the study will have a reference meaning for engineering design, and for providing technical supports for the development of displacement-based seismic design procedure for CLT buildings. However, it is also recommended that further study should focus with a wider scope into the issues related to seismic responses of CLT structures with different archetypes and non-symmetrical floor plans.

Acknowledgements The authors gratefully acknowledge Shanghai Sailing Program (Grant No. 16YF1411800) and Tongji University Civil Engineering International Collaborative Research Fund (Grant No. 0200121005/009) for supporting this research.

References

1. Gavric I, Fragiacomo M, Ceccotti A (2015) Cyclic behavior of typical metal connectors for cross-laminated (CLT) structures. Mater Struct 48:1841–1857
2. Gavric I, Fragiacomo M, Ceccotti A (2015) Cyclic behavior of typical screwed connections for cross-laminated (CLT) structures. Eur J Wood Wood Prod 73:179–191
3. Schneider J, Karacabeyli E, Popovski M, Stiemer SF, Tesfamariam S (2013) Damage assessment of connections used in cross-laminated timber subject to cyclic loads. J Perform Constr Facil 28:A4014008
4. Schneider J, Shen YL, Stiemer SF, Tesfamariam S (2015) Assessment and comparison of experimental and numerical model studies of cross-laminated timber mechanical connections under cyclic loading. Constr Build Mater 77:197–212
5. Ceccotti A, Follesa M, Lauriola MP, Sandhaas C (2006) SOFIE project–test results on the lateral resistance of cross-laminated wooden panels. In: Proceedings of the First European Conf. on Earthquake Engineering and Seismicity, Geneva, Switzerland, Paper 1912
6. Dujic B, Pucelj J, Zarnic R (2004) Testing of racking behavior of massive wooden wall panels. In: Proceedings of the 37th CIB-W18 Meeting, Edinburgh, Scotland, Paper 37-15-2
7. Dujic B, Hristovski V, Stojmanovska M, Zarnic R (2006) Experimental investigation of massive wooden wall panel systems subjected to seismic excitation. In: Proceedings of the First European Conf. on Earthquake Engineering and Seismicity, Zurich, Switzerland
8. Popovski M, Schneider J, Schweinsteiger M (2010) Lateral load resistance of cross-laminated wood panels. In: Proceedings of the 2010 World Conf. on Timber Engineering, Riva del Garda, Italy, Paper 171
9. Ceccotti A, Follesa M (2006) Seismic behavior of multi-storey X-lam buildings. In: COST E29 International Workshop on Earthquake Engineering on Timber Structures, Coimbra, Portugal, pp 1001–1015
10. Ceccotti A, Sandhaas C, Okabe M, Yasumura M, Minowa C, Kawai N (2013) SOFIE project–3D shaking table test on a seven-storey full-scale cross-laminated timber building. Earthq Eng Struct D 42:2003–2021
11. Pei S, Popovski M, van de Lindt JW (2013) Analytical study on seismic force modification factors for cross-laminated timber buildings. Can J Civil Eng 40:887–896
12. Pei S, van de Lindt JW, Popovski M (2012) Approximate R-factor for cross-laminated timber walls in multistory buildings. J Archit Eng 19:245–255
13. Fragiacomo M, Dujic B, Sustersic I (2011) Elastic and ductile design of multi-storey cross-lam massive wooden buildings under seismic actions. Eng Struct 233:3043–3053
14. Latour M, Rizzano G (2017) Seismic behavior of cross-laminated timber panel buildings equipped with traditional and innovative connectors. Arch Civ Mech Eng 17:382–399
15. Mitra N (2012) Pinching4 uniaxial material model (OpenSees online user documentation). http://opensees.berkeley.edu/wiki/index.php/Pinching4_Material. Accessed 20 Dec 2016
16. OpenSees (2016) Open system for earthquake engineering simulation. Pacific Earthquake Engineering Research (PEER) Center, University of California: Berkeley, USA. http://opensees.berkeley.edu/. Accessed 20 Dec 2016
17. Shen YL, Schneider J, Tesfamariam S, Stiemer SF, Mu ZG (2013) Hysteresis behavior of bracket connection in cross-laminated-timber shear walls. Constr Build Mater 48:980–991
18. Park YJ, Ang AS (1985) Mechanistic seismic damage model for reinforced concrete. J Struct Eng ASCE 111:722–739
19. Tesser L, Talledo DA, Corvec VL (2012) ShellMITC4 element (OpenSees online user documentation). http://opensees.berkeley.edu/wiki/index.php/Shell_Element. Accessed 20 Dec 2016
20. Fenves GL (2012) ZeroLength element (OpenSees online user documentation). http://opensees.berkeley.edu/wiki/index.php/ZeroLength_Element. Accessed 20 Dec 2016

21. ASTM E 2126-11 (2011) Standard test methods for cyclic (reversed) load test for shear resistance of walls for buildings. American Society for testing and Materials, West Conshohocken
22. Gavric I, Fragiacomo M, Ceccotti A (2015) Cyclic behavior of CLT wall systems: experimental tests and analytical prediction models. J Struct Eng ASCE 141:04015034
23. Gavric I, Fragiacomo M, Popovski M, Ceccotti A (2014) Behavior of cross-laminated timber panels under cyclic loads. Mater Jt Timber Struct 9:689–702
24. NBCC (2015) National Building Code of Canada 2015. National Research Council of Canada (NRCC), Ottawa
25. Ceccotti A, Sandhaas C (2010) A proposal for a standard procedure to establish the seismic behavior factor q of timber buildings. In: Proceedings of the 2010 World Conf. on Timber Engineering, Riva del Garda, Italy, Paper 834
26. ASCE, SEI 7–10 (2010) Minimum design loads for buildings and other structures. American Society of Civil Engineers, Reston
27. GB 50011–2010 (2010) Code for seismic design of buildings (In Chinese). Ministry of Construction of the People's Republic of China, Beijing
28. Schellenberg A (2012) twoNodeLink element (OpenSees online user documentation). http://opensees.berkeley.edu/wiki/index.php/Two_Node_Link_Element. Accessed 20 Dec 2016
29. GB 50068–2008 (2008) Unified standard for reliability design of building structures (In Chinese). Ministry of Construction of the People's Republic of China, Beijing